THE JOURNAL OF BIOLOGICAL CHEMISTRY VOL. 284, NO. 3, pp. 1863–1872, January 16, 2009
Printed in the U.S.A.

Structural Analysis and Detection of Biological Inositol Pyrophosphates Reveal That the Family of VIP/Diphosphoinositol Pentakisphosphate Kinases Are 1/3-Kinases*[S]

Received for publication, July 24, 2008, and in revised form, October 15, 2008 Published, JBC Papers in Press, November 3, 2008, DOI 10.1074/jbc.M805686200

Hongying Lin[‡], Peter C. Fridy[§], Anthony A. Ribeiro[¶], Jae H. Choi[‖], Deb K. Barma[**], Günter Vogel[‡‡], J. R. Falck[**], Stephen B. Shears[‖], John D. York[§], and Georg W. Mayr[‡1]

From the [‡]Institut für Biochemie und Molekularbiologie I: Zelluläre Signaltransduktion, Universitätsklinikum Hamburg-Eppendorf, Martinistrasse 52, D-20246 Hamburg, Germany, the [§]Howard Hughes Medical Institute, Department of Pharmacology and Cancer Biology, and [¶]NMR Center and Departments of Radiology and Biochemistry, Duke University Medical Center, Durham, North Carolina 27710, the [‖]Inositide Signaling Group, Laboratory of Signal Transduction, NIEHS, National Institutes of Health, Department of Health and Human Services, Research Triangle Park, North Carolina 27709, the [**]Department of Biochemistry, University of Texas Southwestern Medical Center at Dallas, Dallas, Texas 75390, and [‡‡]Fachbereich Mathematik und Naturwissenschaften-Biochemie, Bergische Universität Wuppertal, Gaussstrasse 20, 42097 Wuppertal, Germany

We have characterized the positional specificity of the mammalian and yeast VIP/diphosphoinositol pentakisphosphate kinase (PPIP5K) family of inositol phosphate kinases. We deployed a microscale metal dye detection protocol coupled to a high performance liquid chromatography system that was calibrated with synthetic and biologically synthesized standards of inositol pyrophosphates. In addition, we have directly analyzed the structures of biological inositol pyrophosphates using two-dimensional ^{1}H-^{1}H and ^{1}H-^{31}P nuclear magnetic resonance spectroscopy. Using these tools, we have determined that the mammalian and yeast VIP/PPIP5K family phosphorylates the 1/3-position of the inositol ring *in vitro* and *in vivo*. For example, the VIP/PPIP5K enzymes convert inositol hexakisphosphate to 1/3-diphosphoinositol pentakisphosphate. The latter compound has not previously been identified in any organism. We have also unequivocally determined that 1/3,5-$(PP)_2$-IP_4 is the isomeric structure of the bis-diphosphoinositol tetrakisphosphate that is synthesized by yeasts and mammals, through a collaboration between the inositol hexakisphosphate kinase and VIP/PPIP5K enzymes. These data uncover phylogenetic variability within the crown taxa in the structures of inositol pyrophosphates. For example, in the Dictyostelids, the major bis-diphosphoinositol tetrakisphosphate is 5,6-$(PP)_2$-IP_4 (Laussmann, T., Eujen, R., Weisshuhn, C. M., Thiel, U., Falck, J. R., and Vogel, G. (1996) *Biochem. J.* 315, 715–725). Our study brings us closer to the goal of understanding the structure/function relationships that control specificity in the synthesis and biological actions of inositol pyrophosphates.

Signal transduction pathways frequently rely on a specific target protein recognizing a precise spatial arrangement of one or more phosphate groups on either another protein or a small metabolite. The six-carbon inositol ring offers what is arguably the most dramatic example of how even subtle modifications to phosphate topology can impart signaling specificity. The combinatorial manner in which phosphate groups can be arranged around the inositol skeleton creates a large family of phosphorylated molecules, many of which have individual, physiological roles (1). The inositol pyrophosphates, such as diphosphoinositol tetrakisphosphate (also known as PP-IP_4), PP-IP_5[2] (also known as IP_7) and $(PP)_2$-IP_4 (also known as IP_8) (2, 3), are a specialized subgroup of the inositol-based signaling family that are distinguished by the presence of diphosphate groups. These particular molecules regulate a diverse range of cellular activities, including phosphate sensing, actin cytoskeleton dynamics, apoptosis, vesicle trafficking, transcription, and DNA repair (see Refs. 4 and 5 for reviews). The different isomers of inositol pyrophosphates can be distinguished by biological receptors (6, 7). Thus, there is great interest in understanding the structure/function relationships of protein interactions with the inositol pyrophosphate ligands.

* This work was supported, in whole or in part, by the National Institutes of Health (NIH) Intramural Research Program of the NIEHS (to S. B. S.) and NIH Grants R01 HL-55672 (to J. D. Y.), R01 A1057588 (to A. A. R.), and NCI P30-CA-14236 (to A. A. R.). This research was also supported by the Howard Hughes Medical Institute (to J. D. Y.) and Deutsche Forschungsgemeinschaft Grant MA 989/2-3 (to G. W. M.). Instrumentation in the Duke NMR Center is funded by the National Science Foundation, the NIH, the North Carolina Biotechnology Center, and Duke University. The costs of publication of this article were defrayed in part by the payment of page charges. This article must therefore be hereby marked "*advertisement*" in accordance with 18 U.S.C. Section 1734 solely to indicate this fact.

This paper is dedicated to the late Georg Mayr, Sr., who taught G. W. M. how to address questions experimentally.

[S] The on-line version of this article (available at http://www.jbc.org) contains supplemental material.

[1] To whom correspondence should be addressed. Tel.: 49-40-428033386; E-mail: mayr@uke.uni-hamburg.de.

[2] The abbreviations used are: PP-IP_5, diphosphoinositol pentakisphosphate (also known as IP_7); PPIP5K, PP-IP_5 kinase; $(PP)_2$-IP_4, bis-diphosphoinositol tetrakisphosphate (also known as IP_8); COSY, correlation spectroscopy; GST, glutathione *S*-transferase; HMQC, heteronuclear multiple quantum correlation; HOD, deuterated water; HPLC, high performance liquid chromatography; IP_6, inositol hexakisphosphate; IP6K, IP_6 kinase; MDD, metal dye detection.

Another reason to study the structure of the inositol pyrophosphates is to understand at a molecular level what factors dictate the positional specificity of the kinases and phosphatases that metabolize these polyphosphates. Furthermore, the structure of $(PP)_2$-IP_4 has additional significance, because it can impact the degree of the free energy change during its hydrolysis (8). When one of the diphosphate bonds is cleaved, the ensuing relief of a portion of the electrostatic and steric congestion around the inositol ring will be substantially greater if the pyrophosphates in $(PP)_2$-IP_4 are vicinal (8). This may have practical consequences; the higher the free energy of phosphate hydrolysis, the more thermodynamically favorable it becomes for the phosphate to be transferred to another cellular moiety (8).

In an earlier study (9), chromatographic comparisons of lysates from mammalian cell lines with synthetic PP-IP_5 standards indicated that 5-PP-IP_5 was the major isomer to accumulate. It has, therefore, generally been anticipated that the enzymes that phosphorylate IP_6 to PP-IP_5 would be 5-kinases. One group of these enzymes (IP6Ks; Kcs1 in *Saccharomyces cerevisiae*) was cloned by Snyder and co-workers (10, 11). Recombinant versions of these enzymes were recently used to generate milligram quantities of PP-IP_5 for analysis by one-dimensional (12) and two-dimensional (13) NMR spectroscopy; these experiments confirmed that the IP6Ks are indeed 5-kinases.

Indications that there is a separate class of enzymes capable of phosphorylating IP_6 to PP-IP_5 arose initially from experiments performed on a *kcs1*Δ/*dpp1*Δ double gene deletion strain of *S. cerevisiae* (14). The genes that encode this IP_6 kinase activity have been identified in both *S. cerevisiae* (*Vip1*) (12) and in mammals (*VIP1/PPIP5K1* and *VIP2/PPIP5K2*) (15, 16). These kinases also phosphorylate PP-IP_5 to $(PP)_2$-IP_4 (12, 15, 16). Indeed, the VIP/PPIP5K family appears to account for a distinct PP-IP_5 kinase activity that was observed initially in experiments with cell lysates (17, 18) and subsequently in yeast mutants lacking *Kcs1* (19). Previous one-dimensional ^{31}P NMR studies demonstrated that yeast Vip1 phosphorylates IP_6 to a novel isomer of PP-IP_5 that is different from the 5-PP-IP_5 produced by recombinant human IP6K (12). However, the isomeric nature of this new PP-IP_5 isomer could not be unequivocally established by one-dimensional NMR (it was tentatively suggested to be 4/6-PP-IP_5 (12)). One of the goals of the current study was to unequivocally determine the structure of this novel PP-IP_5 isomer. This is a topic of current interest, because this new isomer regulates the transcriptional activity of a cyclin-cyclin kinase complex in *S. cerevisiae* (6, 7).

It was also our goal to address the lack of information concerning the position of the diphosphate groups on $(PP)_2$-IP_4. The structure of $(PP)_2$-IP_4 has previously only been determined in Dictyostelid cell extracts, since these organisms contain unusually high (300 μM) levels of this compound (20). For example, two-dimensional $^1H/^{31}P$ NMR spectroscopy was used to demonstrate that the $(PP)_2$-IP_4 in *Dictyostelium* cell lysates has one diphosphate group at the 5-position and another at the 4/6-position (21). Another of the Dictyostelids, *Polysphondylium*, also contains 4/6,5-$(PP)_2$-IP_4, plus relatively minor quantities (12–17% of total) of an additional isomer, namely 1/3,5-$(PP)_2$-IP_4 (22). However, it is considerably more challenging to analyze the structures of inositol pyrophosphates in yeast and animal cells, which typically contain only 1–2 μM concentrations of these compounds (23). As a consequence, the structure of $(PP)_2$-IP_4 in mammalian cells has not previously been determined.

In the current study, we have developed a HPLC protocol to routinely identify the structures of the relatively low quantities of the inositol pyrophosphates that are present in most eukaryotic cells. Additionally, in experiments performed *in vitro*, we used recombinant kinases to generate sufficient quantities of $(PP)_2$-IP_4 for unequivocal structural analysis by two-dimensional NMR strategies. We show for the first time that yeast and mammalian VIP/PPIP5K enzymes are 1/3-kinases rather than having the 4/6-kinase activity that was tentatively proposed in an earlier study (12). Thus, the VIP/PPIP5K kinases phosphorylate IP_6 to 1/3-PP-IP_5. Finally, we demonstrate that VIP/PPIP5K enzymes act in concert with IP6K proteins to synthesize $(PP)_2$-IP_4 that has diphosphates at the 5- and 1/3-positions.

EXPERIMENTAL PROCEDURES

Preparation of Synthetic PP-IP_5 and $(PP)_2$-IP_4 Standards—5,6-$(PP)_2$-IP_4 and 1/3,5-$(PP)_2$-IP_4 were isolated from *Dictyostelium* and *Polysphondylium*, respectively, and then purified as previously described (22). The synthesis of the 2,5-$(PP)_2$-IP_4 standard is described in the supplemental material. A mixture of PP-IP_5 and $(PP)_2$-IP_4 standards was prepared by a slight modification of previously published procedures (24, 25). Briefly, a 25-ml reaction was prepared that contained 0.5 mmol of IP_6, 10 mmol of phosphocreatine, and 50 mM NaCl. The pH was adjusted to 3.0 with HCl, and subsequently the mixture was dehydrated by overnight freeze-drying. The freeze-dried material was resuspended in 200 ml of water, and the mixture of PP-IP_5/$(PP)_2$-IP_4 isomers were purified by Q-Sepharose chromatography.

Preparation of Biological Isomers of PP-IP_5 and $(PP)_2$-IP_4—Several different enzyme preparations were used to prepare inositol pyrophosphates for analysis by MDD-HPLC. In one series of experiments, $(PP)_2$-[^{3}H]IP_4 was prepared from full-length recombinant forms of human FLAG-tagged VIP1/PPIP5K1 and, separately, from human FLAG-tagged VIP2/PPIP5K2, both of which were expressed and immunopurified as described previously (15). These enzymes were individually incubated with approximately 4000 dpm of PP-[^{3}H]IP_5 (15) in 50–200 μl of a medium that was designed to maximize product yield from an impure enzyme preparation (*e.g.* it included an ATP regeneration system and NaF to inhibit phosphatase activity (26)): 1 mM EDTA, 50 mM KCl, 20 mM HEPES, pH 7.0, 12 mM $MgSO_4$, 10 mM NaATP, 20 mM phosphocreatine, 0.04 mg/ml creatine kinase, 0.6 mg/ml bovine serum albumin, 1 mM dithiothreitol, and 10 mM NaF. Reactions were quenched by boiling (4 min).

In a separate series of experiments, $(PP)_2$-IP_4 was prepared by incubating IP_6 with full-length recombinant human GST-IP6K1, plus either GST fusion constructs comprising residues 1–387 of the human VIP1/PPIP5K1 kinase domain or residues 1–535 of the *Sc*Vip1 kinase domain; all of these enzymes were bacterially expressed and purified as previously described (12,

16). The incubation buffer contained 50 mM HEPES (pH 6.2), 50 mM NaCl, 5 mM $MgCl_2$, 30 mM phosphocreatine, 50 units of creatine kinase, 5 mM ATP, and 200 μM IP_6. Reactions were quenched by boiling (10 min). Parallel reactions were performed with 2- [^{32}P]IP_6 to monitor the progress of the reactions (16).

PP-IP_5 for NMR was prepared using recombinant GST-tagged *Sc*Vip1 kinase domain. In a 5-ml reaction, 10 μmol of IP_6 was incubated with 375 μg of GST-*Sc*Vip1 in buffer containing 50 mM HEPES (pH 7.0), 50 mM NaCl, 1.5 mM ATP, 3 mM $MgCl_2$, 24 mM creatine phosphate, and 250 units of creatine kinase. After 16 h at 37 °C, the reaction was boiled for 10 min, and 350 μl of 1.5 M Tris-HCl (pH 8.8) was added along with 60 μl of 0.5 M EDTA (pH 8.0). The sample was centrifuged (12 min at 4,100 rpm), and the supernatant was passed through a 0.22-μm filter. The sample was then loaded onto a Mono Q HR 5/5 column (GE Life Sciences) and run with the following gradient: 0–10 min, 100% buffer A (0.2 mM HCl, 1 mM EDTA (pH 8.0)); 10–40 min, linear gradient 0–100% buffer B (0.5 M HCl, 1 mM EDTA (pH 8.0)); 40–60 min, 100% buffer B. A flow rate of 1.0 ml/min was used, and 1-ml fractions were collected. The fractions that contained inositol phosphates were identified as described previously (12), neutralized with 5 M KOH, and lyophilized. The lyophilized product was resuspended in 1 ml of 99.96% D_2O. $(PP)_2$-IP_4 for NMR analysis was prepared using recombinant GST-tagged *Sc*Vip1 kinase domain and full-length human IP6K1. In a 5-ml reaction, under conditions described above, 10 μmol of IP_6 was incubated with 375 μg of GST-*Sc*Vip1 and 100 μg of GST-IP6K1 for 16 h at 37 °C. Samples were quenched, HPLC-purified, and resuspended in 1 ml of 99.96% D_2O as described above.

NMR Analysis—NMR spectra were obtained at 300 K using a Varian Inova 500 NMR spectrometer equipped with a Dell Precision 390 work station and a 5-mm Varian probe. Proton and phosphorus chemical shifts are reported relative to external tetradeutero sodium propionate and undiluted H_3PO_4 at 0.00 ppm. The ^{2}H signal of D_2O was used as a field frequency lock.

One-dimensional 500 MHz ^{1}H NMR spectra were obtained with a 1600 Hz spectral window, a 45° pulse field angle (3.6 μs), a 6.4-s acquisition time, and a 1-s relaxation delay. The spectra were digitized using 20,484 points to obtain a digital resolution of 0.156 Hz/point. The HOD signal was suppressed by a selective presaturation pulse. The one-dimensional ^{1}H NMR spectra were plotted onto F_2 and F_1 of the ^{1}H-^{1}H two-dimensional spectra and onto F_2 of the ^{1}H-^{31}P two-dimensional spectra. The HOD solvent signal reproducibly occurred at 4.784 ppm on the tetradeutero sodium propionate scale.

^{1}H-decoupled ^{31}P NMR spectra were recorded at 202.3 MHz with a spectral window of 12,143.3 Hz digitized into 96,000 data points (digital resolution of 0.253 Hz/point), a 60° pulse flip angle (20 μs), and a 4.96-s total repeat time. Inverse decoupled difference spectra were recorded as ^{1}H-detected ^{31}P-decoupled heteronuclear NMR experiments, as previously described (27, 28).

Metal Dye Detection (MDD) HPLC Analysis—MDD-HPLC was performed on a MiniQ PC 3.2/3 column (Amersham Biosciences) using a Kontron system (BioTEK) as described previously (29) with a slight modification to reduce analysis time and increase sensitivity. Thus, 1–5 nmol of a mixture of standards (see below) or sample was dissolved in 1–1.2 ml of 2 mM sodium acetate plus 2 mM NaF and injected using an autosampler (Kontron AS560). Two different gradients were employed in the current study by mixing buffer A (0.2 mM HCl, 15 μM YCl_3) with buffer B (0.5 M HCl, 15 μM YCl_3). Gradient 1 was as follows: 0–2 min, 3–45% B; 2–2.5 min, 45–58% B; 2.5–2.8 min, 58–59% B; 2.8–9 min, 59–65% B; 9–12.5 min, 65–80% B; 12.5–13 min, 80–100% B; 13–16 min, 100% B; and 16.1–20 min, 3% B. Gradient 2 was as follows: 0–1 min, 3% B; 1–2 min, 3–50% B; 2–2.5 min, 50–58% B; 2.5–3 min, 58–59% B; 3–10 min, 59–60% B; 10–10.6 min, 60–65% B; 10.6–13.5 min, 65–80% B; 13.5–17 min, 80–100% B; 17–18.5 min, 100% B; and 18.6–23 min, 3% B. The flow rate was 0.5 ml/min.

The eluate from the column was mixed in-line with half of the volume of a buffer containing 300 μM 4-(2-pyridylazo)resorcinol in 1.6 M triethanolamine (pH 9.0 with HCl), and the degree of the postcolumn complexometric reaction was recorded by measuring absorbance at 546 nm (SPD-10Avvp; Shimadzu). Data were stored in a polarity-switched format (multiplied by −1) and exported into Sigmaplot for imaging. All samples were routinely mixed with our mixture of standards (see above) and rechromatographed; in no case did this cause any changes to the elution time of any of the peaks in the standards. In some experiments (gradient 2 only), the YCl_3 was omitted from the elution buffers; the 4-(2-pyridylazo)resorcinol was replaced by water; and 20 s fractions were collected and mixed with 2 ml of INSTA-GEL scintillant (Packard), and radioactivity was determined using liquid scintillation spectrometry.

Cell Culture and Extraction of Inositol Phosphates—NIH-Swiss 3T3 cells, H1299 cells, and MDA cells were all maintained in Dulbecco's modified Eagle's medium (Invitrogen) with 10% fetal bovine serum (Sigma) in 5% CO_2 at 37 °C on 15-cm Petri dishes to about 70% confluence. Cells were treated with either vehicle or 10 mM NaF for 2 h. Subsequently, cells were rinsed with ice-cold phosphate-buffered saline and scraped into ice-cold lysis buffer (8% (w/v) trichloroacetic acid, 10 mM EDTA), followed by twice freezing and thawing in liquid nitrogen. After no more than 30 min, the precipitate was removed by centrifugation (3500 × *g* for 10 min at 4 °C), and the supernatants were extracted three times with 3 ml of water-saturated diethyl ether. After the pH had been adjusted to about 6 with Tris (0.5 M), the extract was concentrated in a SpeedVac.

RESULTS AND DISCUSSION

Phylogenetic Differences in Inositol Pyrophosphate Structure—The ability to separate and quantify inositol phosphates and inositol pyrophosphates is critically important for understanding cellular metabolism and signaling regulatory networks. The recent increased interest in the biology of inositol pyrophosphates (4) has made it especially important to determine the structures of each species within this diverse array of molecules. For example, Albert *et al.* (9) previously employed a MDD HPLC method for resolving different isomers of PP-IP_5. We have now further developed the MDD-HPLC protocol for routine separation of $(PP)_2$-IP_4 isomers.

To calibrate our chromatography system, a mixture of PP-IP_5 and $(PP)_2$-IP_4 isomers were prepared in "shotgun" fashion

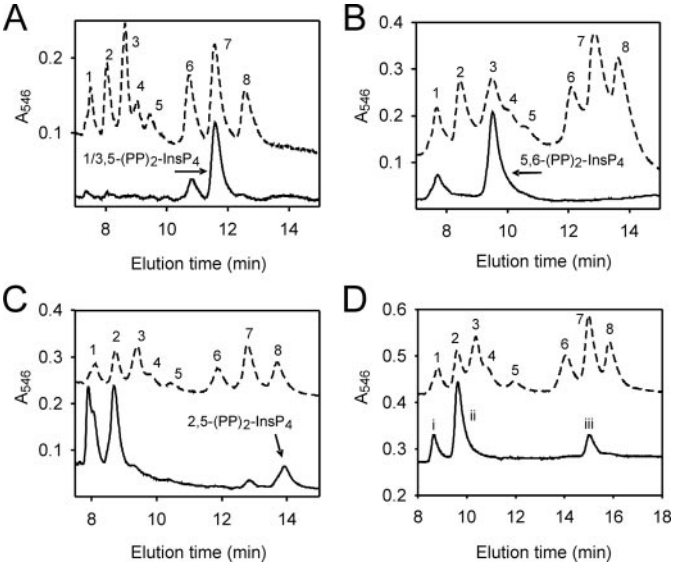

FIGURE 1. **Analysis of $(PP)_2$-IP_4 isomers by MDD-HPLC.** Either 1 nmol of NMR-defined standards of 1/3,5-$(PP)_2$-IP_4 from *Polysphondylium* (*A*, *lower trace*), 2.5 nmol of NMR-defined standards of 5,6-$(PP)_2$-IP_4 from *Dictyostelium* (*B*, *lower trace*), or 2.3 nmol of chemically synthesized 2,5-$(PP)_2$-IP_4 (*C*, *lower trace*) were separated by MDD-HPLC (gradient 1). *D* shows the PP-IP_5 and $(PP)_2$-IP_4 produced (*lower trace*) when both human GST-IP6K1 (5 μg) and GST-*Sc*Vip1 kinase domain (50 μg) were incubated with 100 nmol of IP_6 in 3-h reactions performed at 37 °C as described under "Experimental Procedures"; 10-μl aliquots (~2 nmol of total inositol (pyro)phosphate) were taken for analysis. Gradient 2 was used in the MDD-HPLC analysis. Each *panel* also includes the elution of a mixture of standards (about 10 nmol) from a parallel HPLC run (*upper*, *broken line* in each *panel*). *Peaks 1* and *2* represent the elution positions of PP-IP_5 isomers, and *peaks 3–8* represent the elution positions of $(PP)_2$-IP_4 isomers (for details, see "Results"). Each sample elution position relative to the standard mixture was also verified by co-chromatography of sample and standards (data not shown) in separate runs. The slight differences in the elution times of the different peaks within the standard mixture reflect column-to-column variation during the 4-year period in which these data were obtained.

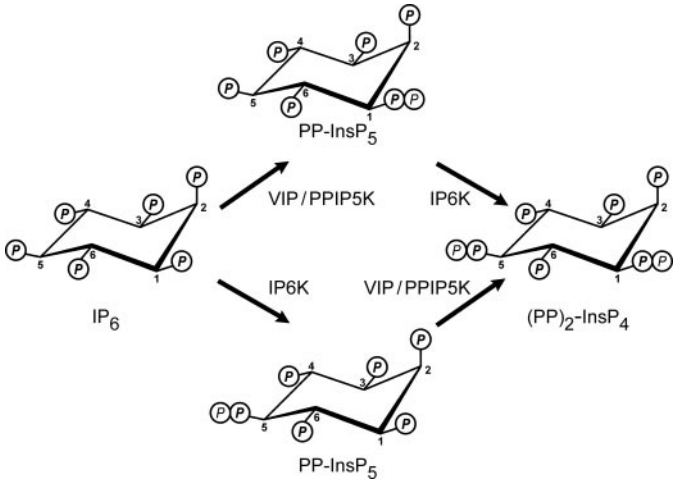

FIGURE 2. **The products of IP_6 phosphorylation in yeast and mammals.** The graphic shows the products of IP_6 phosphorylation that are characterized in the current study. Note that we have depicted the lowest numbered of the two possible locants for the 1/3-diphosphate group; stereoselective analysis will be required to determine which of these two alternatives is formed.

from IP_6 by a nonenzymatic, dehydration-driven transphosphorylation reaction that used creatine phosphate as a phosphate donor (see "Experimental Procedures"). This mixture was resolved by MDD-HPLC into eight different peaks that eluted after IP_6 (*labeled 1–8* in Fig. 1). There was some column-to-column variability in the absolute elution positions of the various peaks (compare *A*, *B*, and *C* in Fig. 1, which include data obtained at various times during a 4-year period). Nevertheless the elution pattern of our standard mixture was highly reproducible. Peak 1 contains 4/6-PP-IP_5 and a leading shoulder of 5-PP-IP_5, and peak 2 contains 1/3-PP-IP_5 and 2-PP-IP_5; these elution positions were verified by calibrating the HPLC system with chemically synthesized standards of each of these individual PP-IP_5 isomers (9, 22, 25, 30). The remaining six peaks represent the elution positions of $(PP)_2$-IP_4 isomers. For example, we found that peak 7 in our mixture of synthetic standards (Fig. 1*A*) corresponded to the elution position of a two-dimensional NMR-characterized standard of 1/3,5-$(PP)_2$-IP_4 (from *Polysphondylium* (22)). Peak 3 (Fig. 1*B*) corresponded to the elution position of a standard of 5,6-$(PP)_2$-IP_4 (from *Dictyostelium* (22, 30)). Peak 8 in our synthetic mixture corresponded to the elution position of a chemically synthesized standard of 2,5-$(PP)_2$-IP_4 (Fig. 1*C*; decomposition of this particular standard to PP-IP_5 was noted).

It has previously (12, 15, 16, 31) been determined that the IP6K and VIP/PPIP5K enzymes work in concert to generate $(PP)_2$-IP_4. Thus, when IP_6 was incubated with both human IP6K and *Sc*Vip1, three products accumulated (*labeled peaks i*, *ii*, and *iii* in Fig. 1*D*). Peak i co-eluted with the PP-IP_5 product that was formed when IP_6 was phosphorylated by human IP6K alone (data not shown; this material has previously been validated by NMR to be 5-PP-IP_5 (13)). Peak ii co-eluted with the PP-IP_5 product that was formed when IP_6 was incubated with yeast Vip1 alone (data not shown); this PP-IP_5 coeluted with a synthetic 1/3-PP-IP_5 standard (data not shown), and in addition it was validated by NMR to be 1/3-PP-IP_5 (see below). Peak iii contains the $(PP)_2$-IP_4 that was formed in these experiments, and this co-eluted with peak 7 of our standard mixture (Fig. 1*D*). This is also the elution point for a two-dimensional NMR-characterized 1/3,5-$(PP)_2$-IP_4 standard from *Polysphondylium* (Fig. 1*A*). These HPLC data provide the first evidence that *Sc*Vip1 is a 1/3-kinase (and see Fig. 2).

Is the positional specificity of Vip1 from yeast conserved in mammals? To answer this question, we next characterized the nature of the $(PP)_2$-IP_4 produced from 5-PP-IP_5 upon its phosphorylation by full-length, recombinant human VIP1/PPIP5K1 (Fig. 3*A*) and, in separate assays, VIP2/PPIP5K2 (Fig. 3*B*). These enzymes were expressed in HEK cells with an N-terminal FLAG epitope for subsequent immunopurification. For these experiments, we incubated each of the purified kinases with ^{3}H-labeled 5-PP-IP_5 (Fig. 3). The possible products of this reaction were 4/6,5-$(PP)_2$-IP_4 (equivalent to peak 3 in our standard mixture), 2,5-$(PP)_2$-IP_4 (peak 8), and 1/3,5-$(PP)_2$-IP_4 (peak 7). The only $(PP)_2$-IP_4 product to accumulate was 1/3,5-$(PP)_2$-IP_4 (Fig. 3). In further experiments, we also incubated IP_6 with IP6K plus the catalytic domain of human VIP1/PPIP5K1 that was expressed in *Escherichia coli*; MDD-HPLC analysis indicated that 1/3,5-$(PP)_2$-IP_4 was again the only isomer of $(PP)_2$-IP_4 to accumulate (data not shown). These results indicate that the mammalian VIP/PPIP5K enzymes have the same positional specificity as their yeast homologue.

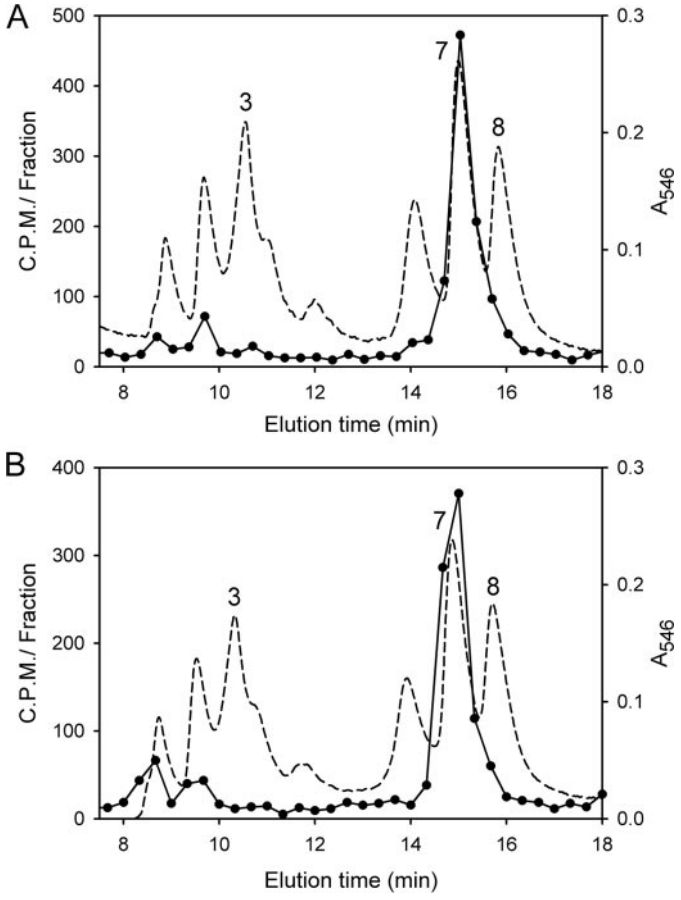

FIGURE 3. **MDD-HPLC analysis of the $(PP)_2$-IP_4 produced by phosphorylation of 5-PP-IP_5 by human VIP/PPIP5K types 1 and 2.** 5-PP-[^{3}H]IP_5 was incubated with either 750 ng of immunopurified human FLAG-VIP1/PPIP5K1 in 200 μl of assay buffer for 2 h (*A*) or 225 ng of immunopurified human FLAG-VIP2/PPIP5K2 in 50 μl of assay buffer for 1 h (*B*). Assays were quenched and analyzed by MDD-HPLC using gradient 2. Fractions were collected every 20 s. A mixture of standards (*broken lines*) was separated in parallel runs; *peak 3* corresponds to 4/6,5-$(PP)_2$-IP_4, *peak 7* corresponds to 1/3,5-$(PP)_2$-IP_4, and *peak 8* corresponds to 2,5-$(PP)_2$-IP_4 (see other figures and "Results" for explanation).

Analysis of the Structures of IP_6, PP-IP_5, and $(PP)_2$-IP_4 by Two-dimensional NMR—Provided that milligram quantities of pure inositol phosphates can be prepared, NMR can be used to analyze their structure (32, 33). We used ^{31}P and ^{1}H one- and two-dimensional NMR analysis to determine the structures of the two inositol pyrophosphates (PP-IP_5 and $(PP)_2$-IP_4) produced by the VIP1/PPIP5K family (see "Experimental Procedures" and Fig. 3). HPLC-purified IP_6 was also used as a standard. The ^{1}H-decoupled ^{31}P NMR spectrum of IP_6 at pH 6 (Fig. 4*A*) reveals ^{31}P signals at 2.82, 1.93, and 1.54 ppm in the ratio 1:2:3, corresponding to six phosphate signals. A 1:2:2:1 pattern was previously observed at pH 11 (21) and is expected from equivalence of the P-1/3 and P-4/6 pairs due to the symmetry of the inositol ring along an axis through positions 2 and 5. The IP_6 spectrum at pH 6 is explained by merging of the upfield single phosphate signal with the upfield double phosphate signal. The ^{31}P NMR spectrum of PP-IP_5 (Fig. 4*B*), in contrast, reveals five individual phosphate singlets (2.91, 2.00, 1.66, 1.41, and 0.73 ppm) and two pyrophosphate doublets (−7.95 and −9.77 ppm, J_{PP} = 20.4 Hz). The five distinct singlets indicate that the PP-IP_5 molecule no longer possesses the axis of symmetry, indicating that a pyrophosphate group is added at either position 1, 3, 4, or 6. The ^{31}P NMR spectrum of $(PP)_2$-IP_4 (Fig. 4*C*) reveals four individual phosphate singlets (1.87, 1.57, 1.20, and 0.57 ppm) and four pyrophosphate doublets (−7.90, −8.04, −9.24, and −9.62 ppm, J_{PP} = 20.4 and 18.7 Hz). This ^{31}P NMR spectrum is ambiguous for positional assignments, and we therefore turned to ^{1}H NMR.

The ^{1}H NMR spectrum of our IP_6 standard at pH 6.0 (Fig. 4*D*) reveals a distinct double-triplet near 5.03 ppm, a two-proton quartet near 4.53 ppm, and three proton resonances that overlap near 4.28 ppm. The 5.03 ppm double-triplet is assigned to H-2, since this is the sole equatorial proton on the inositol ring, and will be shifted downfield relative to the five other protons that are in axial positions (33). The 9.5 Hz splitting is identified as a proton-phosphorus coupling (J_{HP}) from ^{31}P decoupling experiments (see below and Fig. 6). The 2.4 Hz splitting is recognized as the equatorial-axial coupling from H-2 to H-1/3 (J_{12} and J_{32}). Two of the three resonances at 4.27 ppm show triple-triplet line shape with 2 Hz axial-equatorial coupling, indicating that these arise from H-1 and H-3. These resonances are chemically equivalent due to the axis of symmetry through positions 2 and 5. The two-proton quartet with large proton-phosphorus coupling (~9 Hz) and axial-axial proton-proton coupling (~9 Hz) likewise must be chemically equivalent H-4 and H-6 resonances due to the symmetry axis. The remaining one-proton quartet at 4.28 ppm with large proton-phosphorus and axial-axial couplings is therefore assigned as H-5. Comparison with the reported IP_6 spectrum at pH 5 (33) confirmed assignment of the 5.03 ppm double-triplet to H-2. In the previously described IP_6 spectrum at pH 5 (33), the chemically equivalent H-1 and H-3 triple-triplets appear at a chemical shift of ~4.21 ppm (scale corrected from HOD solvent signal at 4.67 ppm to HOD at 4.784 ppm) and overlap almost completely with the H-5 quartet. This accords with the spectrum of our IP_6 standard at pH 6, in which the H-1, H-3, and H-5 resonances overlap at 4.27 ppm. This leaves the remaining two-proton quartet signal near 4.53 ppm assigned to H-4 and H-6.

Subsequent comparison of the ^{1}H NMR spectra of the kinase products with the IP_6 spectrum allows deductions on the ring positions of the pyrophosphate groups. The ^{1}H NMR spectrum of PP-IP_5 (Fig. 4*E*) shows the double-triplet near 5.08 ppm (H-2), two overlapped multiplets near 4.55 ppm (H-4/6), a resolved triple-triplet near 4.37 ppm (H-1/3), and an overlapped quartet at 4.31 ppm (H-5) and a hidden triple-triplet at 4.29 ppm (H-1/3) (Fig. 4). The 4.37 ppm triple-triplet features the small (~2 Hz) equatorial-axial coupling and is assigned as either H-1 or H-3, whereas the 4.31 ppm quartet features only large proton-phosphorus and axial-axial couplings and is assigned as H-5. Since the resolved triple-triplet (4.37 ppm) is well shifted from the hidden triple-triplet (4.28 ppm), the PP-IP_5 very likely has its pyrophosphate group at the 1- or 3-position. NMR cannot further distinguish between these two alternatives, due to the symmetry axis of the inositol ring.

The ^{1}H NMR spectrum of $(PP)_2$-IP_4 (Fig. 4*F*) reveals the H-2 double-triplet near 5.07 ppm, two overlapped multiplets near 4.63 ppm (H-4/6), a distinct quartet near 4.48 ppm, and two resolved triple-triplets at 4.43 and 4.33 ppm. The two triple-triplets with the ~2 Hz couplings are clearly the H-1/3 pair,

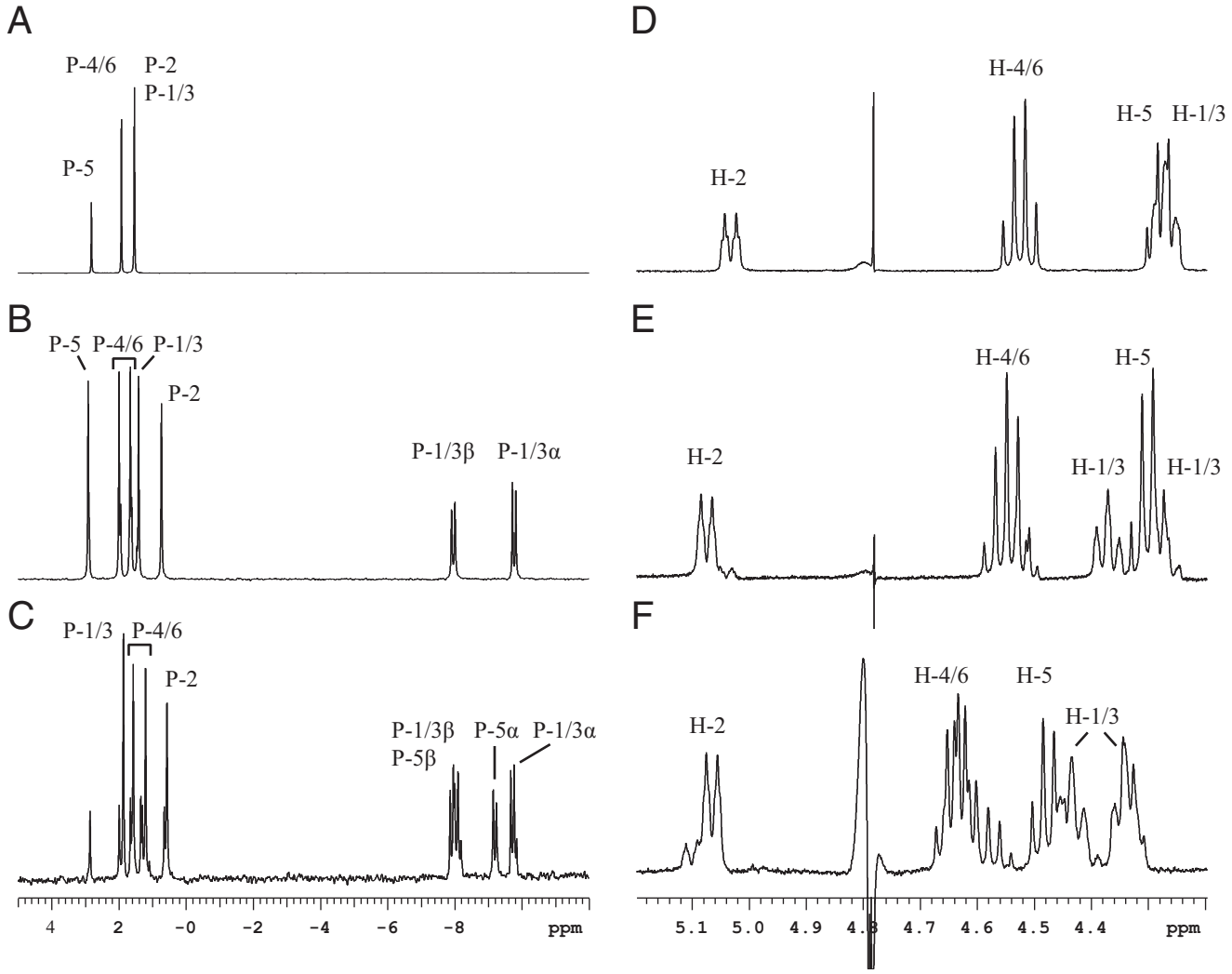

FIGURE 4. **NMR spectroscopy at pH 6 of IP_6, $PP\text{-}IP_5$, and $(PP)_2\text{-}IP_4$.** *A*, the ^1H-decoupled ^{31}P NMR spectrum of IP_6. *B*, the ^{31}P NMR spectrum of $PP\text{-}IP_5$. *C*, the ^{31}P NMR spectrum of $(PP)_2\text{-}IP_4$. Approximately 20% of the total signal arises from unreacted $PP\text{-}IP_5$. *D*, the ^1H NMR spectrum of IP_6. *E*, the ^1H NMR spectrum of $PP\text{-}IP_5$. The shoulder resonances (<10%) arise from IP_6. *F*, the ^1H NMR spectrum of $(PP)_2\text{-}IP_4$. The additional side peaks (~20%) arise from $PP\text{-}IP_5$.

leaving the 4.48 ppm quartet to be assigned to H-5. Thus, the $(PP)_2\text{-}IP_4$ probably has its pyrophosphate groups at the 1/3- and 5-positions.

The ^1H NMR assignments of the chemically distinct protons on the inositol ring of IP_6, $PP\text{-}IP_5$, and $(PP)_2\text{-}IP_4$ were all further confirmed by two-dimensional COSY (21, 22, 33) and are discussed here only for $(PP)_2\text{-}IP_4$. COSY cross-peaks from the H-2 double-triplet (5.07 ppm) assign the 4.33 and 4.43 ppm proton multiplets as the H-1/3 peak pairs. The latter each show cross-peaks to two proton multiplets at 4.64 ppm, thus assigning the 4.64 ppm resonances to H-4 and H-6. The H-4/6 multiplets in turn show a cross-peak with the quartet at 4.47 ppm, which is confirmed as H-5 (22, 33).

With ^1H NMR assignments at hand, two-dimensional $^1H\text{-}^{31}P$ HMQC spectra were pursued to obtain ^{31}P NMR assignments. HMQC for IP_6 (Fig. 5*A*) revealed cross-peaks from the 4.28 ppm quartet (H-5) to the single phosphorus signal at 2.82 ppm (P-5), from the 2-proton quartet at 4.53 ppm (H-4/6) to the two-phosphorus signal at 1.93 ppm (P-4/6), and from the 5.03 ppm double-triplet (H-2) and equivalent 4.27 ppm triple-triplets (H-1/3) to the three-phosphorus signal at 1.54 ppm. HMQC for $PP\text{-}IP_5$ (Fig. 5*B*) reveals the α-pyrophosphate peak at −9.77 ppm to show a prominent cross-peak with the previously assigned H-1/3 ^1H peak (4.37 ppm), confirming that the pyrophosphate group on $PP\text{-}IP_5$ is at the 1- or 3-position. The H-2 ^1H double-triplet (5.07 ppm) shows a distinct HMQC cross-peak to the 0.73 ppm ^{31}P signal, assigning it to P-2. The H-4/6 multiplets (4.55 ppm) show connectivities to the 2.00 and 1.66 ppm ^{31}P signals, assigning these as the P-4/6 pairs. The H-5 quartet (4.30 ppm) shows a cross-peak to the 2.92 ppm ^{31}P signal, assigning it to P-5. The remaining H-1/3 peak (4.29 ppm) correlates to the remaining ^{31}P signal at 1.41 ppm as a P-1/3 peak. HMQC for $(PP)_2\text{-}IP_4$ (Fig. 5*C*) shows the α-pyrophosphate peaks at −9.24 and −9.62 ppm with strong cross-peaks to the previously assigned H-1/3 and H-5 ^1H peaks, confirming that the pyrophosphate groups on $(PP)_2\text{-}IP_4$ are at the 5- and 1- or 3-positions. The H-2 ^1H double-triplet (5.07 ppm) shows a distinct HMQC cross-peak to the 0.57 ppm ^{31}P signal, assigning it to P-2. The H-4/6 multiplets (4.64 ppm) show connectivities to the 1.57 and 1.20 ppm ^{31}P signals,

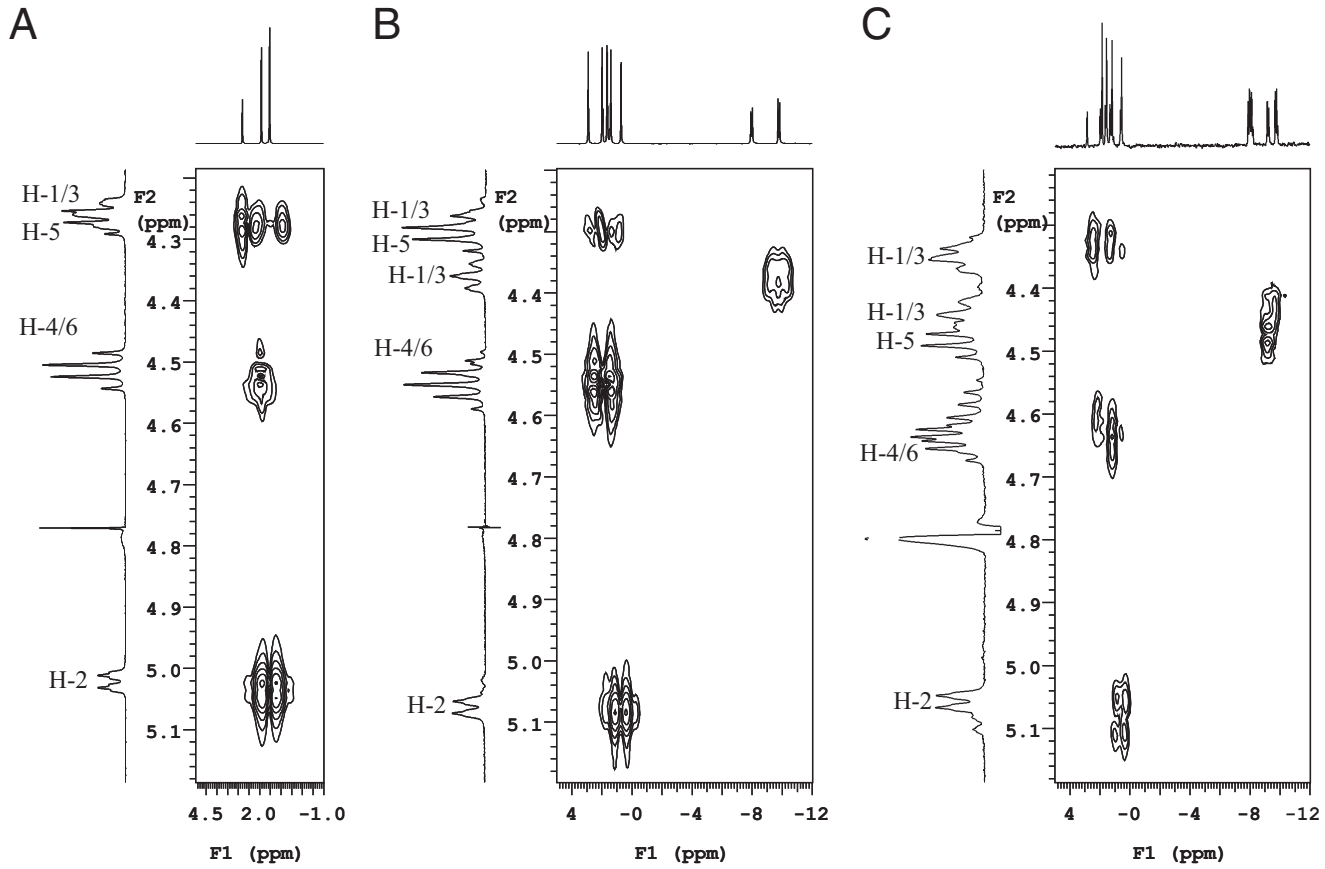

FIGURE 5. **Two-dimensional ^{1}H-^{31}P HMQC spectra at pH 6 of IP$_6$, PP-IP$_5$, and (PP)$_2$-IP$_4$.** *A*, IP$_6$; *B*, PP-IP$_5$; *C*, (PP)$_2$-IP$_4$. Singlet monophosphate peaks that could not be unequivocally assigned from the two-dimensional spectra were assigned by selective ^{31}P-decoupled ^{1}H spectra.

assigning these as the P-4/6 pairs. The remaining H-1/3 peak (4.33 ppm) correlates to the remaining ^{31}P signal at 1.81 ppm as a P-1/3 peak.

Two additional decoupling strategies employing highly digitized one-dimensional spectra were then pursued. These experiments remove interpretative ambiguities from limited resolution in the two-dimensional data and allowed direct measurement of the relevant coupling constants. In the first strategy, one-dimensional ^{1}H NMR spectra incorporating selective ^{31}P decoupling were collected and are illustrated first for IP$_6$ and second for (PP)$_2$-IP$_4$ (Fig. 6). Selective decoupling of the 1.54 ppm three-phosphate ^{31}P signal of IP$_6$ (P-2; P-1 and P-3) (Fig. 6*A*) removes the phosphorus-proton coupling (9.9 Hz) and simplifies the double-triplet (5.03 ppm; H-2) to a simple triplet with axial-equatorial coupling (2.4 Hz) and the triple-triplet to a double-triplet (4.27 ppm; H-1 and H-3) with axial-axial and axial-equatorial couplings. Selective decoupling of the 1.93 ppm two-phosphate ^{31}P signal (P-4/6) (Fig. 6*B*) removes the phosphorus-proton coupling (9.5 Hz) and leaves a simplified triplet at 4.53 ppm (H-4/6) with axial-axial proton-proton couplings. Similarly, selective decoupling of the 2.82 single ^{31}P signal (P-5) (Fig. 6*C*) pinpoints the location of a ^{1}H triplet (H-5) at 4.27 ppm with axial-axial proton-proton couplings (9.5 Hz). Selective decoupling of the 0.57 ppm ^{31}P signal (P-2) of (PP)$_2$-IP$_4$ (Fig. 6*E*) removes the phosphorus-proton coupling (9.9 Hz) and simplifies the double-triplet (H-2) to a simple triplet, with small axial-equatorial coupling (2.4 Hz). The splittings of the other proton peaks are not affected, and subtraction of a control spectrum gives complete cancellation in the 4.3–4.7 ppm region of the difference spectrum (data not shown). Selective decoupling of the 1.87 ppm ^{31}P signal (P-1/3) removes the phosphorus-proton coupling (9.5 Hz) and leaves a simplified double-triplet at 4.33 ppm (H-1/3) with proton-proton couplings of 9.5 and 2.4 Hz. Similarly, selective decoupling of the 1.57 and 1.20 ppm ^{31}P signals (P-6 and P-4) pinpoints the location of ^{1}H triplets at 4.629 and 4.641 ppm, respectively, with large axial-axial proton-proton couplings (9.5 Hz). Selective decoupling of the −9.24 ppm ^{31}P signal (P-5α) collapses the 4.473 ppm quartet (H-5) to a triplet with 10.5 Hz proton-proton coupling. Selective decoupling of the −9.62 ppm ^{31}P signal (P-1/3α) collapses the 4.43 ppm complex triplet (H-3/H-1) into a "doublet" with one large proton-proton coupling (9.4 Hz) and an unresolved proton-proton coupling (2.4 Hz).

In the second strategy, one-dimensional ^{31}P NMR spectra with selective ^{1}H decoupling were collected and are only discussed for (PP)$_2$-IP$_4$ (spectra not shown). The ^{1}H-coupled ^{31}P NMR spectrum reveals doublets for each phosphomonoester signal and double-doublets for each pyrophosphate signal. Selective ^{1}H decoupling of the 5.07 ppm ^{1}H signal (H-2) removes the large phosphorus-proton coupling (9.87 Hz) and simplifies the 0.57 ppm ^{31}P doublet (P-2) to a singlet with no other changes in the ^{31}P NMR spectrum. The splittings of the other phosphorus peaks are unaffected, and subtraction of a control spectrum gives complete cancellation in all other

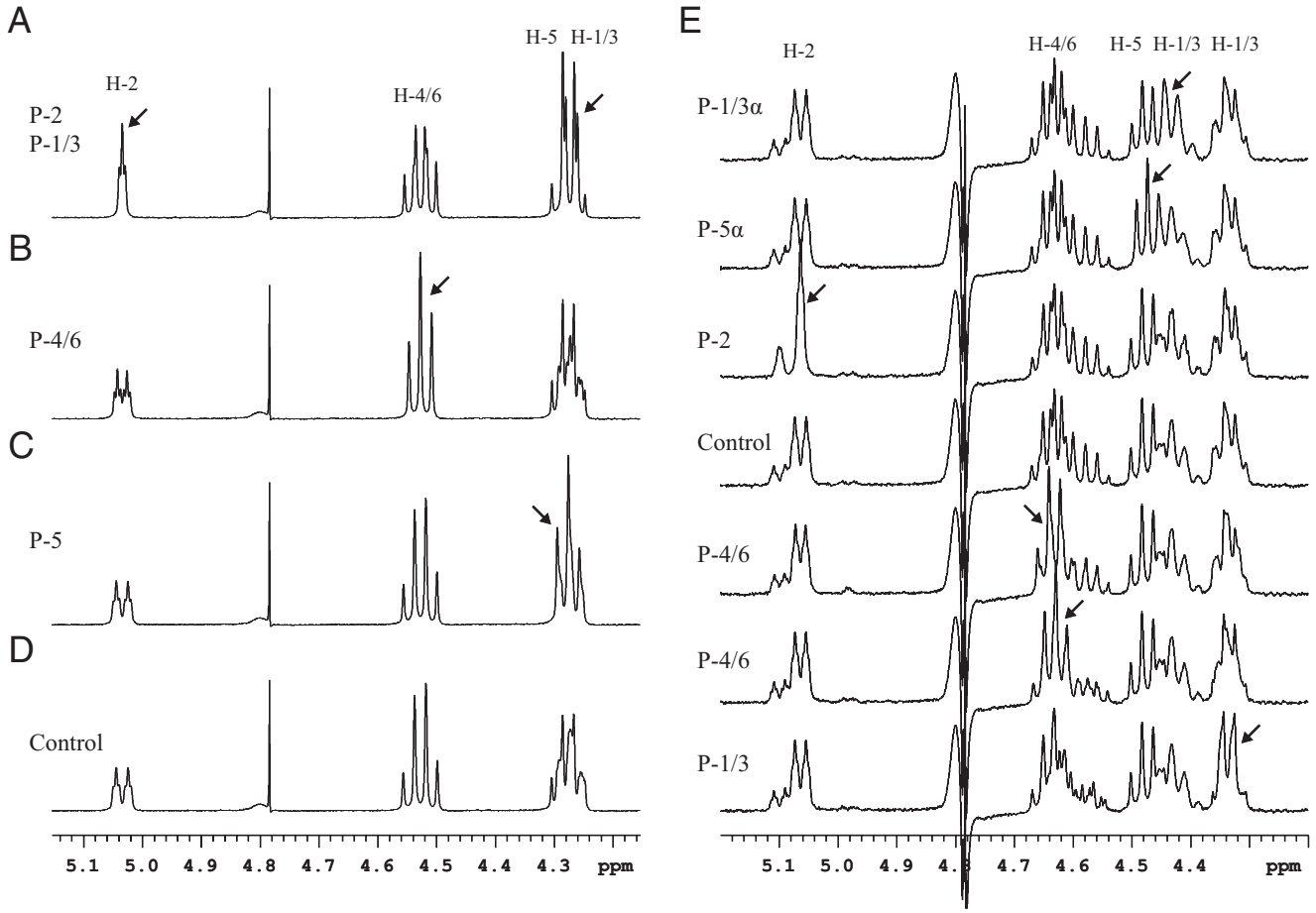

FIGURE 6. **^{31}P-decoupled ^{1}H NMR spectra of IP_6 (*A–D*) and $(PP)_2$-IP_4 (*E*).** *A–C*, IP_6 spectra with selective ^{31}P decoupling at the 1.54, 1.93, and 2.82 resonances; *D*, a control spectrum with off-resonance decoupling. *E*, ^{1}H NMR spectra were collected as before, with the addition of selective inverse decoupling, where for each spectrum, a specific phosphorus peak was irradiated, eliminating its coupling from the ^{1}H spectrum. From *top* to *bottom*, the phosphorus chemical shifts used for decoupling are −9.72 ppm, −9.19 ppm, 0.57 ppm, 25 ppm (off resonance control with no ^{31}P peak decoupled), 1.20 ppm, 1.57 ppm, and 1.87 ppm. Assignment of ^{1}H peaks was based on two-dimensional ^{1}H-^{1}H COSY spectrum (not shown). The ring position of the phosphorus decoupled in each spectrum was then inferred from the assigned position of the proton peak with reduced coupling (*arrows*). See "Results" for discussion.

TABLE 1
NMR data at pH 6 for IP_6

Position	δH	$^{3}J_{H\text{-}H}$ [a]	δP	$^{3}J_{P\text{-}H}$ [b]
	ppm	*Hz*	*ppm*	*Hz*
1/3	4.272	2.4, 9.9	1.536	9.5
2	5.034	2.4	1.536	10.2
3/1	4.272	2.4, 9.9	1.536	10.0
4/6	4.527	9.9	1.925	9.7
5	4.276	9.4	2.317	10.5
6/4	4.527	9.9	1.925	9.7

[a] Error in coupling constant from one-dimensional ^{1}H NMR data is 0.16 Hz.
[b] Error in coupling constant from one-dimensional ^{31}P NMR data is 0.25 Hz.

TABLE 2
NMR data at pH 6 for PP-IP_5

Position	δH	$^{3}J_{H\text{-}H}$ [a]	δP	$^{3}J_{P\text{-}H}$ [b]	$^{2}J_{P\text{-}P}$ [b]
	ppm	*Hz*	*ppm*	*Hz*	*Hz*
1/3	4.286	2.4, 9.3	1.412	9.5	
2	5.077	2.4	0.733	9.9	
3/1α	4.374	2.4, 9.4	−9.766	10.0	20.4
3/1β			−7.954		20.4
4/6	4.561	9.4	1.660	9.9	
5	4.305	9.4	2.914	10.5	
6/4	4.541	9.4	1.997	9.2	

[a] Error in coupling constant from one-dimensional ^{1}H NMR data is 0.16 Hz.
[b] Error in coupling constant from one-dimensional ^{31}P NMR data is 0.25 Hz.

TABLE 3
NMR data at pH 6 for $(PP)_2$-IP_4

Position	δH	$^{3}J_{H\text{-}H}$ [a]	δP	$^{3}J_{P\text{-}H}$ [b]	$^{2}J_{P\text{-}P}$ [b]
	ppm	*Hz*	*ppm*	*Hz*	*Hz*
1/3	4.338	2.4, 9.3	1.865	9.5	
2	5.065	2.4	0.567	9.9	
3/1α	4.432	2.4, 9.4	−9.621	10.0	20.0
3/1β			−8.041		20.0
4/6	4.641	9.4	1.204	9.9	
5α	4.473	9.4	−9.244	10.5	18.7
5β			−7.701		18.7
6/4	4.629	9.4	1.568	9.2	

[a] Error in coupling constant from one-dimensional ^{1}H NMR data is 0.16 Hz.
[b] Error in coupling constant from one-dimensional ^{31}P NMR data is 0.25 Hz.

regions of the difference spectrum (data not shown). Selective ^{1}H decoupling of the two overlapped 4.64 ppm ^{1}H multiplets (H-6 and H-4) similarly simplifies the 1.20 and 1.57 ^{31}P doublets (P-6 and P-4) to singlets. Selective decoupling of the 4.33 ppm complex triplet (H-3/H-1) collapses the 1.865 ppm ^{31}P doublet to a singlet (P-3/P-1). Selective decoupling of the 4.47 ppm quartet (H-5) collapses the −9.24 ppm ^{31}P double-doublet to a doublet (P-5α). Selective decoupling of the 4.43 ppm triple-triplet (H-1/3) collapses the −9.62 ppm ^{31}P double-doublet to a

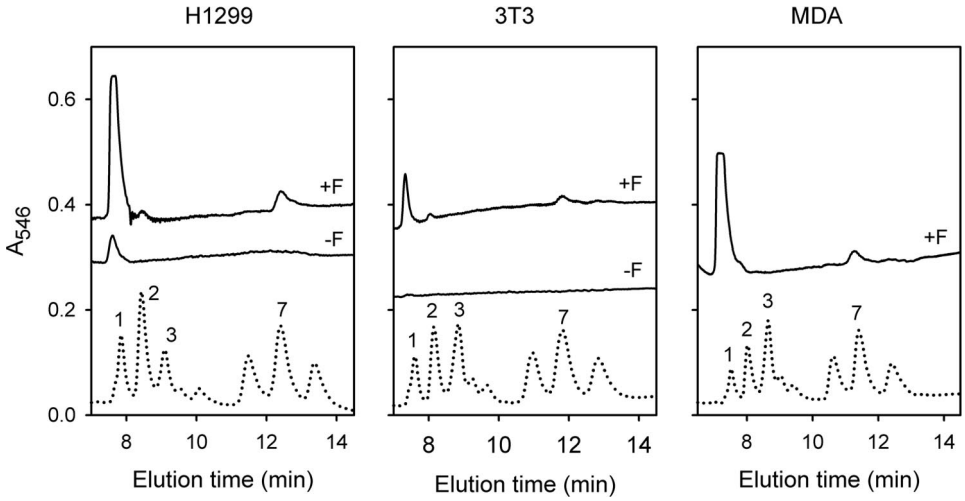

FIGURE 7. **MDD-HPLC analysis of PP-IP_5 and $(PP)_2$-IP_4 in mammalian cell lines.** Either H1299, 3T3, or MDA cells were incubated with either vehicle or 10 mM NaF for 2 h. Cell lysates were prepared and analyzed by MDD-HPLC (*solid lines*) using gradient 1. A mixture of standards was chromatographed in parallel. *Peak 1* marks the elution position of 4/6-PP-IP_5 and 5-PP-IP_5; *peak 2* marks the elution position of 1/3-PP-IP_5 and 2-PP-IP_5. *Peak 3* corresponds to 4/6,5-$(PP)_2$-IP_4, and *peak 7* corresponds to 1/3,5-$(PP)_2$-IP_4 (for explanation, see the other figures and "Results").

doublet (P-1/3α). The derived NMR assignments and coupling constant data are summarized in Tables 1–3.

The complex splitting patterns of the peaks seen in the one-dimensional ^{1}H spectra can now be understood. Consideration of the large couplings observed from the proton-phosphorus and axial-axial proton-proton interactions (^3J about 9 Hz) leads to predictable doublet, triplet, and quartet peaks at the H-2, H-1/3, and H-4/H-5/H-6 positions, respectively. The presence of the smaller coupling (2.4 Hz) adds fine splittings at the H-2 and H-1/3 positions, resulting in the "small triplets," as expected from previous studies (33). The results of the two decoupling strategies corroborate and validate the HMQC and COSY NMR data, reinforcing our conclusion that the $(PP)_2$-IP_4 has its pyrophosphate groups at the 1/3- and 5-positions.

One final point to emerge from these NMR experiments was the absence of any signals indicating that a triphosphate was formed (the estimated limit of detection is 2% of total products). This finding indicates another difference between the VIP/PPIP5K family and the IP6K family, in that the latter can convert IP_6 to a limited quantity of the triphosphate, 5-PPP-$InsP_5$, at least *in vitro* (13).

Analysis of $(PP)_2$-IP_4 in Mammalian Cells—We have used MDD-HPLC to investigate if the spectrum of $(PP)_2$-IP_4 isomers in mammalian cells corresponded to the 1/3-positional specificity of the VIP/PPIP5K family that we have characterized *in vitro*. It is difficult to detect inositol pyrophosphates in lysates prepared from less than 100 mg of wet packed weight of mammalian cells (Fig. 7), as reported previously (9). However, we did observe significant quantities of PP-IP_5 in H1299 cells (Fig. 7); this inositol pyrophosphate co-eluted with peak 1 of our standard mixture and is probably 5-PP-IP_5 (9). We next used a pharmacological approach to elevate cellular levels of inositol pyrophosphates to more readily detectable levels; we treated cells with 10 mM NaF for 2 h. Fluoride inhibits the phosphatases that normally rapidly metabolize the inositol pyrophosphates (3, 9, 26). This explains why the treatment of cells with NaF substantially increased the levels of 5-PP-IP_5 (Fig. 7). A second effect of NaF was to promote the appearance of an additional isomer of PP-IP_5 that co-eluted with peak 2 from our standard mixture. This is probably 1/3-PP-IP_5, produced by phosphorylation of IP_6 by VIP/PPIP5K. This use of NaF has therefore unmasked an ongoing flux through this metabolite *in vivo*. In three different cell types, the NaF treatment also caused a single $(PP)_2$-IP_4 peak to accumulate (Fig. 7). Its co-elution with peak 7 from our standard mixture is consistent with this material being 1/3,5-$(PP)_2$-IP_4 (*e.g.* see Fig. 1*A*). These experiments verify the significance *in vivo* of the $(PP)_2$-IP_4 product that we have defined to be produced *in vitro* by the VIP/PPIP5K class of inositol phosphate kinases.

General Conclusions—The universality and versatility of inositol-based signaling owes much to the wealth of second messengers that are synthesized by combinatorial phosphorylation of the six hydroxyl groups that are situated around the inositol ring. In the current study, we characterize a new aspect of this diversity by determining the spatially specific placement of pyrophosphate groups by the VIP/PPIP5K family. We report that the yeast and mammalian VIP/PPIP5K proteins are 1/3-kinases, thereby contributing to the synthesis of 1/3-PP-IP_5 and 1/3,5-$(PP)_2$-IP_4 *in vivo*. This finding is significant for a number of reasons.

First, we find that yeast and mammals do not synthesize 5,6-$(PP)_2$-IP_4, which is the exclusive isomer of $(PP)_2$-IP_4 in several species of slime molds (21, 22) and the major isomer (>80% of total $(PP)_2$-IP_4) in others (two species of *Polysphondylium*). The pattern of PP-IP_5 isomers in *Dictyostelium* (5-PP-IP_5 and 6-PP-IP_5 (22) also differs from that in mammalian cells (5-PP-IP_5 and 1/3-PP-IP_5; see above). In fact, our work represents the first identification of the presence of 1/3-PP-IP_5 in any organism. These phylogenetic differences are especially intriguing when considering that many of the mammalian inositol lipids and inositol phosphates are conserved in slime molds. Indeed, phylogenetic analysis has placed the Dictyostelids in the so-called "crown taxa" that includes green plants, fungi, and animals (34). Nevertheless, our data now suggest that previous (35) use of *Dictyostelium* as a model system for probing mechanisms of actions of inositol pyrophosphates may not actually be applicable to mammalian cells.

Second, the vicinal diphosphate groups in 5,6-$(PP)_2$-IP_4 give this molecule a significantly higher standard free energy of hydrolysis than the 1/3,5-PP-IP_5 in yeast and mammalian cells (8). This may provide slime molds with a more energetically efficient donor molecule for transphosphorylation reactions,

such as those that directly phosphorylate certain proteins, *in vitro* at least (36, 37).

Third, the availability of the structure of both $(PP)_2$-IP_4 (this study) and DIPP1 (Protein Data Bank entry 2FVV) provides new opportunities to understand some enigmatic aspects of this hydrolase activity. For example, modeling of substrate into the active site may help us understand why the positional specificity of DIPP varies depending upon whether $(PP)_2$-IP_4 or PP-IP_5 is the substrate (17). This modeling might also help explain why F84Y and H91L mutations in DIPP specifically compromise $(PP)_2$-IP_4 hydrolysis but leave PP-IP_5 hydrolysis largely unaffected (38). The increased understanding of the structures of inositol pyrophosphates described in the current study will also help us understand the structural basis for their synthesis by the VIP/PPIP5K family. The determination that the VIP/PPIP5K enzymes synthesizes 1/3-PP-IP_5 and not the 4/6-isomer that had previously been tentatively assumed (6, 12) places us one substantial step closer to understanding the structural determinants of ligand specificity for the regulation by PP-IP_5 of the transcriptional activity of a cyclin-cyclin-dependent kinase complex that controls cellular phosphate accumulation (6, 7).

Finally, our studies also represent a significant step forward to the goal of the chemical synthesis of physiologically relevant isomers of inositol pyrophosphates and the development of structurally based inhibitors of the metabolism and action of this class of molecules. This is likely to be a field of growing interest, since evidence that the inositol pyrophosphates are important cellular regulators continues to accumulate (4).

Acknowledgments—We thank Melanie Eckhard and Karsten Lindner for synthesizing the mixture of PP-IP_5 and $(PP)_2$-IP_4 standards.

REFERENCES

1. Irvine, R. F., and Schell, M. (2001) *Nat. Rev. Mol. Cell Biol.* **2,** 327–338
2. Stephens, L. R., Radenberg, T., Thiel, U., Vogel, G., Khoo, K.-H., Dell, A., Jackson, T. R., Hawkins, P. T., and Mayr, G. W. (1993) *J. Biol. Chem.* **268,** 4009–4015
3. Menniti, F. S., Miller, R. N., Putney, J. W., Jr., and Shears, S. B. (1993) *J. Biol. Chem.* **268,** 3850–3856
4. Bennett, M., Onnebo, S. M., Azevedo, C., and Saiardi, A. (2006) *Cell Mol. Life Sci.* **63,** 552–564
5. Onnebo, S. M., and Saiardi, A. (2007) *Cell* **129,** 647–649
6. Lee, Y. S., Huang, K., Quiocho, F. A., and O'Shea, E. K. (2008) *Nat. Chem. Biol.* **4,** 25–32
7. Lee, Y. S., Mulugu, S., York, J. D., and O'Shea, E. K. (2007) *Science* **316,** 109–112
8. Hand, C. E., and Honek, J. F. (2007) *Bioorg. Med. Chem. Lett.* **17,** 183–188
9. Albert, C., Safrany, S. T., Bembenek, M. E., Reddy, K. M., Reddy, K. K., Falck, J. R., Bröker, M., Shears, S. B., and Mayr, G. W. (1997) *Biochem. J.* **327,** 553–560
10. Saiardi, A., Erdjument-Bromage, H., Snowman, A., Tempst, P., and Snyder, S. H. (1999) *Curr. Biol.* **9,** 1323–1326
11. Saiardi, A., Nagata, E., Luo, H. R., Snowman, A. M., and Snyder, S. H. (2001) *J. Biol. Chem.* **276,** 39179–39185
12. Mulugu, S., Bai, W., Fridy, P. C., Bastidas, R. J., Otto, J. C., Dollins, D. E., Haystead, T. A., Ribeiro, A. A., and York, J. D. (2007) *Science* **316,** 106–109
13. Draskovic, P., Saiardi, A., Bhandari, R., Burton, A., Ilc, G., Kovacevic, M., Snyder, S. H., and Podobnik, M. (2008) *Chem. Biol.* **15,** 274–286
14. York, S. J., Armbruster, B. N., Greenwell, P., Petes, T. D., and York, J. D. (2005) *J. Biol. Chem.* **280,** 4264–4269
15. Choi, J. H., Williams, J., Cho, J., Falck, J. R., and Shears, S. B. (2007) *J. Biol. Chem.* **282,** 30763–30775
16. Fridy, P. C., Otto, J. C., Dollins, D. E., and York, J. D. (2007) *J. Biol. Chem.* **282,** 30754–30762
17. Shears, S. B., Ali, N., Craxton, A., and Bembenek, M. E. (1995) *J. Biol. Chem.* **270,** 10489–10497
18. Huang, C.-F., Voglmaier, S. M., Bembenek, M. E., Saiardi, A., and Snyder, S. H. (1998) *Biochemistry* **37,** 14998–15004
19. Choi, K., Mollapour, E., and Shears, S. B. (2005) *Cell. Signal.* **17,** 1533–1541
20. Laussmann, T., Pikzack, C., Thiel, U., Mayr, G. W., and Vogel, G. (2000) *Eur. J. Biochem.* **267,** 2447–2451
21. Laussmann, T., Eujen, R., Weisshuhn, C. M., Thiel, U., Falck, J. R., and Vogel, G. (1996) *Biochem. J.* **315,** 715–725
22. Laussmann, T., Hansen, A., Reddy, K. M., Reddy, K. K., Falck, J. R., and Vogel, G. (1998) *FEBS Lett.* **426,** 145–150
23. Ingram, S. W., Safrany, S. T., and Barnes, L. D. (2003) *Biochem. J.* **369,** 519–528
24. Mayr, G. W., Radenberg, T., Thiel, U., Vogel, G., and Stephens, L. R. (1992) *Carbohydr. Res.* **234,** 247–262
25. Lin, H. Y., Lindner, K., and Mayr, G. W. (2009) in *Methods in Molecular Biology: Inositol Phosphates and Lipids* (Barker, C. J., ed), Humana Press Inc., Totowa, NJ
26. Safrany, S. T., Caffrey, J. J., Yang, X., Bembenek, M. E., Moyer, M. B., Burkhart, W. A., and Shears, S. B. (1998) *EMBO J.* **17,** 6599–6607
27. Ribeiro, A. A., Zhou, Z., and Raetz, C. R. H. (1999) *Magn. Reson. Chem.* **37,** 620–631
28. Zhou, Z., Ribeiro, A. A., and Raetz, C. R. (2000) *J. Biol. Chem.* **275,** 13542–13551
29. Mayr, G. W. (1988) *Biochem. J.* **254,** 585–591
30. Laussmann, T., Reddy, K. M., Reddy, K. K., Falck, J. R., and Vogel, G. (1997) *Biochem. J.* **322,** 31–33
31. Otto, J. C., Kelly, P., Chiou, S. T., and York, J. D. (2007) *Proc. Natl. Acad. Sci. U. S. A.* **104,** 15653–15658
32. Scholz, P., Bergmann, G., and Mayr, G. W. (1990) in *Methods in Inositide Research* (Irvine, R. F., ed) Raven Press, New York
33. Johnson, K., Barrientos, L. G., Le, L., and Murthy, P. P. (1995) *Anal. Biochem.* **231,** 421–431
34. Baldauf, S. L., and Doolittle, W. F. (1997) *Proc. Natl. Acad. Sci. U. S. A.* **94,** 12007–12012
35. Luo, H. R., Huang, Y. E., Chen, J. C., Saiardi, A., Iijima, M., Ye, K., Huang, Y., Nagata, E., Devreotes, P., and Snyder, S. H. (2003) *Cell* **114,** 559–572
36. Bhandari, R., Saiardi, A., Ahmadibeni, Y., Snowman, A. M., Resnick, A. C., Kristiansen, T. Z., Molina, H., Pandey, A., Werner, J. K., Jr., Juluri, K. R., Xu, Y., Prestwich, G. D., Parang, K., and Snyder, S. H. (2007) *Proc. Natl. Acad. Sci. U. S. A.* **104,** 15305–15310
37. Saiardi, A., Bhandari, A., Resnick, R., Cain, A., Snowman, A. M., and Snyder, S. H. (2004) *Science* **306,** 2101–2105
38. Yang, X., Safrany, S. T., and Shears, S. B. (1999) *J. Biol. Chem.* **274,** 35434–35440